JOURNAL OF GEOPHYSICAL RESEARCH, VOL. 101, NO. B3, PAGES 5507–5517, MARCH 10, 1996

Marine controlled-source electromagnetic sounding 1. Modeling and experimental design

Á. H. Flosadóttir[1] and S. Constable
Scripps Institution of Oceanography, University of California San Diego, La Jolla

Abstract. Numerical forward modeling, predicting an observable response given a mathematical representation of the Earth, is an important component of practical exploration work. In addition, derivatives which relate changes in response to changes in the Earth model are useful for experimental design and are a crucial element of linearized inversion techniques. Differentiation of kernels followed by numerical integration using a fast Hankel transform provides an efficient combination of forward and sensitivity modeling for frequency-domain horizontal electric dipole-dipole sounding over a layered seafloor. Our code is validated against an independent forward modeling technique using a mode analysis and against central difference derivatives. Efficiency is important in the application of regularized inversion to large data sets; we give an example from the East Pacific Rise, requiring 2000 elements in the Jacobian matrix. We illustrate the use of forward modeling and discrete analogs of the Fréchet kernels to provide aid to physical intuition and experimental design in the context of the electrical conductivity of the oceanic lithosphere. By using the most favorable parts of range-frequency space, experiments using current technology should be capable of distinguishing a thicker, less resistive, from a thinner, more resistive "lithospheric resistor" layer.

Introduction

The electrical conductivity profile of normal oceanic lithosphere and uppermost asthenosphere still provides a subject of lively debate. In addition to the intrinsic geophysical interest in this problem, for example to establish limits on the oceanic lithosphere's water content and the submarine asthenosphere's melt content, this issue is of considerable technical importance for magnetotelluric data interpretation and possibly for the interpretation of motionally induced voltages in terms of large-scale ocean circulation.

The seafloor horizontal electric dipole-dipole (HED) controlled source method has been instrumental in demonstrating the existence of highly resistive lithosphere at several locations under the ocean basins [*Young and Cox*, 1981; *Cox et al.*, 1986]. In this pair of papers, we use both sensitivity and experimental studies to address some further contributions of this method to the problem of the crust and uppermost mantle's conductivity profile. The present paper gives the necessary background on the experimental method and presents our computational method, an efficient combination of forward and derivative modeling for the HED experimental configuration over a one-dimensional seafloor. We test various aspects of our code, illustrate it in regularized inversion of a small seafloor data set, and demonstrate how insights obtained from forward and sensitivity modeling can be used in experimental design. In particular, we attempt to outline the limits of this method's deep sensitivity. Seafloor controlled-source measurements, as well as magnetotelluric studies using the TM (transverse magnetic) mode near coastlines, suggest that the lithospheric mantle has a transverse resistance (resistivity–thickness product) of around 10^9 Ω m^2 [*Cox et al.*, 1986; *Mackie et al.*, 1988]. Natural-source soundings have characteristically assigned conductivities of between 0.1 and 0.01 S/m, or higher, to the uppermost mantle in the depth range 50–150 km (a recent review is given by *Tarits*, [1994]). *Heinson and Constable* [1992] noted that these conductivities are far higher than those obtained in laboratory experiments on subsolidus olivine and mantle rocks. Assuming a uniformly resistive lithosphere, they obtained numerical modeling results which supported a previous suggestion that the coast effect can severely affect marine magnetotelluric (MT) responses even far from coastlines [*Cox*, 1980; *Ranganayaki and Madden*, 1980]. The numerical results indicated that this effect would bias one-dimensional (1-D) marine MT interpretations in favor of underlying conductive layers, and *Heinson and Constable* [1992] suggested that this might account for the discrepancy between the laboratory results and the traditional data interpretation. On the other hand, so might a percentage of partial melts or a variety of trace materials. *Tarits et al.* [1993] demonstrated that by assuming conductive pathways between ocean basins and underlying conductors, the coast effect was reduced by about a decade, although the resulting electric field was still significantly smaller than in the case without coastlines. The size of the effect, of course, depends on the conductance of the pathways assumed. Each position in the ensuing debate as to both reliability of one-dimensional interpretation of marine MT data and the presence of a submarine "electrical asthenosphere" [*Tarits et al.*, 1993; *Constable and Heinson*, 1993] has a degree of

[1]Now at Pacific Marine Environmental Laboratory, NOAA, Seattle, Washington.

Paper number 95JB03739.
0148-0227/96/95JB-03739$05.00.

self-consistency, and independent experimental evidence would clearly provide the most unequivocal resolution. The high resistivity of the lithosphere is extremely poorly sensed in one-dimensional MT experiments, and resistivity and thickness are highly correlated parameters in higher dimensional (TM-mode) MT soundings. Resistivity and thickness are also difficult to decouple in controlled-source work. In our sensitivity study, we ask whether the resistivity and thickness of the most resistive layer can be sensed separately, and whether the presence or absence of an electrical asthenosphere can be extracted in the presence of realistic ambient noise and other experimental limitations. The companion paper [*Constable and Cox*, this issue] presents the results of the PEGASUS experiment, where the method was applied to 40-Ma-old lithosphere in the northeast Pacific in an attempt to address these issues.

Experimental Method

In order to measure electrical conductivity in any material an electric or electromagnetic field is applied and its attenuation observed. The natural, time-varying electromagnetic field of Earth has been used extensively to investigate Earth's mantle under the oceans (e.g., reviews by *Cox et al.* [1971], *Filloux* [1987], and *Tarits* [1994]). However, attenuation of high-frequency components on passage through the water column, motion of the sensors by water currents, and contamination by motional induction of conductive seawater flowing through Earth's magnetic field, all serve to limit the bandwidth.

An artificial electromagnetic field, as long as it is generated on or close to the seafloor, can replace the higher-frequency components that are attenuated in the natural field by the overlying seawater. Controlled-source marine electromagnetic (EM) sounding methods [*Cox*, 1980; *Edwards et al.*, 1981] consist of transmitting time-varying electromagnetic signals between two points, most often located at or near the seafloor. For an introduction to recent experimental work, see reviews by *Constable* [1990], *Chave et al.* [1991], and recent papers by *Webb et al.* [1993], *Evans et al.* [1994], and *Constable and Cox* [this issue]. The theory has been developed extensively in both one- and two-dimensional structures with and without anisotropy [*Chave and Cox*, 1982; *Chave*, 1984; *Edwards and Chave*, 1986; *Flosadóttir*, 1990; *Yu and Edwards*, 1992; *Everett and Edwards*, 1993; *Unsworth*, 1994; *Unsworth and Oldenburg*, 1995]. *Jattieva et al.* [1993] attempted to show that the spatial character of the signal contains more information on the distribution of electrical conductivity of the rocks below the sea than the variation with frequency. This is only approximately true, as our sensitivity study will show, but in practice, attenuation of high-frequency signals by conductive seafloor and corruption of low-frequency signals by magnetotelluric noise limits the usable bandwidth to about 2 decades between 0.01 and 10 Hz.

In addition to the higher-frequency content, the controlled-source method contrasts with the marine MT method in other useful ways. It is highly sensitive to buried resistive layers, provided the attenuation on passage through overlying layers is not too great. Furthermore, the much smaller scale of the source fields makes distant Earth features such as coastlines and topography less likely to complicate a local interpretation. The sensitivity to buried resistive layers can also provide a very useful complement to seismic methods. Many materials which are relatively resistive in the context of porous sediments, among them basalts, ice, massive carbonates, and evaporites, tend to be opaque to seismic methods. Controlled-source surveying thus offers a complementary technique in areas where seismic reflection techniques perform poorly, such as sediments overlain by basalts or carbonates, regions of permafrost, and some salt dome structures.

We will restrict this paper to the horizontal electric dipole-dipole (HED) frequency domain sounding configuration used by the groups with which the authors have been associated at Scripps Institution of Oceanography (SIO) and Cambridge University (Figure 1). This system uses a seafloor horizontal electric dipole source to inject an electromagnetic signal into the ocean basement. Energy propagating through the rock leaks back up into the ocean and is detected by a series of horizontal electric field receivers. The experimental system has been described in part by *Webb et al.* [1985], *Constable* [1990], *Chave et al.* [1991], *Sinha et al.* [1990], and in the companion paper [*Constable and Cox*, this issue]. A variant developed to complement seismic methods of structural mapping in the context of oil and mineral exploration on the continental shelf consists of towing source and receiver in tandem [*Constable et al.*, 1986].

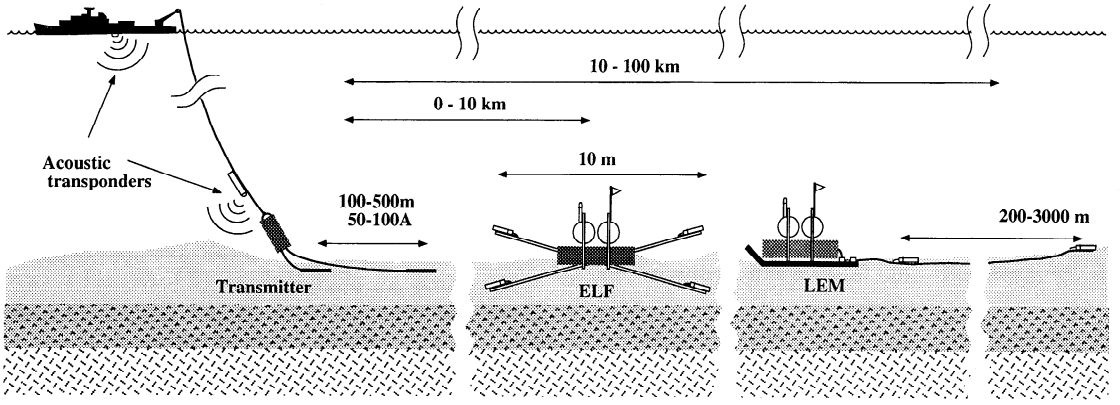

Figure 1. Diagram of the horizontal electric dipole-dipole (HED) frequency domain sounding configuration. A dipole transmitter is towed on, or close to, the seafloor while recording voltmeters measure electric fields that have propagated through the seabed. The most easily deployed instrument is an electric field instrument with an orthogonal pair of 10 m antennas (ELF), but greater signal to noise ratios can be achieved by deploying a longer cable using the long-wire electromagnetic instrument (LEM).

Computation

Numerical modeling is a necessary component of practical exploration work. In principle, finite difference and finite element methods can model arbitrary sources and three-dimensional structure. Although the higher-dimensional methods developed for the marine controlled-source method in the last few years [*Everett and Edwards*, 1989; *Flosadóttir*, 1990; *Unsworth et al.*, 1993] have not yet been used for inversion of multidimensional field data, the numerical capability appears to be within reach [*Unsworth and Oldenburg*, 1995]. However, there is still a role for one-dimensional computation. The relative uniformity of large tracts of sea floor and the effort required to collect extensive data sets in the marine environment mean that situations continue to exist where data are not collected in sufficient quantity to constrain multidimensional interpretation. One-dimensional modeling is also useful as a check of multidimensional methods. It can handle long ranges and deeply penetrating signals that require finite difference or element model domains so large as to tax current computational capabilities. Last but not least, the power of simple models as an aid to physical intuition and sensitivity studies should not be underestimated. The relative simplicity of one-dimensional models and the ease and speed of calculation invite a more thorough exploration of the model and data spaces than might be the case with more complex models.

The combined forward and sensitivity computation method described in this paper has been in use for analysis of the data obtained by the SIO and Cambridge experimental groups for the past several years [*Evans et al.*, 1991, 1994; *Constable and Cox*, this issue]. It is based on the forward-only code of *Chave and Cox* [1982], which computed the seafloor horizontal electric field as a numerically integrated continuum of Fourier-Bessel wavenumbers, that is, a Hankel transform. The wavenumber domain response is constructed by recursion up through a stack of seabed layers, starting from a boundary condition in an underlying half-space. *Ghosh* [1971] introduced a rapid digital filtering approach to evaluating such transforms in the specific case of Schlumberger resistivity sounding. Provided source-receiver ranges are not too large (the integrand's oscillatory nature eventually overcomes any numerical integration method), such methods are very suitable for the solution of the seafloor dipole-dipole problem. The code of Chave and Cox provided both a fast Hankel transform (FHT) [*Anderson*, 1979] and an alternative method by *Chave* [1983]. By employing the much slower method of Gaussian quadrature between Bessel function zeroes and using Padé approximants to force convergence, this method was designed to work to relatively longer ranges than the FHT.

Table 1. Conductivity Models for Sensitivity Study

	Layer	Depth	Model R σ, S/m	Model C σ, S/m
Seawater	0	0 km	3.2	3.2
Sediments	1	40 m	0.3	0.3
Extrusives	2	700 m	0.1	0.1
Intrusives	3	6 km	10^{-3}	10^{-3}
Mantle	4	36 km	1.63×10^{-5}	10^{-5}
Mantle	5	55 km	1.63×10^{-5}	3.0×10^{-3}
Mantle	6	75 km	3.0×10^{-4}	3.0×10^{-3}
Mantle	7	100 km	10^{-3}	3.0×10^{-2}
Mantle	8		10^{-2}	0.1

Two models representative of a hot, dry, resistive upper mantle (R for resistive) and relatively conductive upper mantle (C for conductive). The most resistive layer in model R has been split into two sublayers in order to facilitate layer-by-layer comparison with model C. Depths are to the base of each layer, and the seawater layer is 5 km thick.

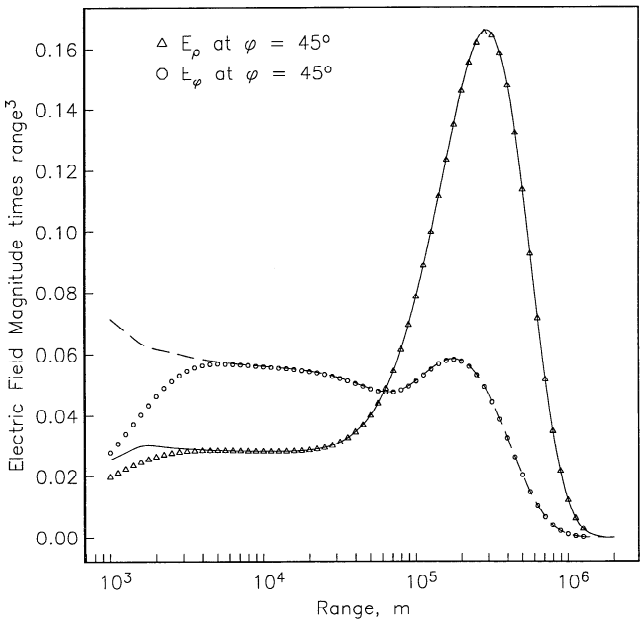

Figure 2. Forward computation compared with the independent computational method of *Flosadóttir* [1990]. The magnitude of the radial and azimuthal electric field components have been multiplied by r^{-3} (r in m), then plotted as functions of source-receiver distance r along a line at a 45° angle with the transmitter axis. The Earth model is model C of Table 1. The calculation assumes an HED source of unit strength operating at 1 Hz. The solid and broken lines are computed with the combined sensitivity-forward code, using the fast Hankel transform. Symbols are computed with a normal-mode expansion using 30 modes of each polarization. The mode expansion breaks down at ranges less than about 5 km.

The advent of inversion for smoothly layered models [*Constable et al.*, 1987; *Smith and Booker*, 1988], and the increasingly large data sets resulting from work with towed sources and multiple stationary receivers, prompted us to develop a more efficient computational method. In our version of Chave and Cox's method, we have simplified and improved the forward performance by implementing the use of *Anderson's* [1989] hybrid Hankel transform code, published after an interchange of ideas on the relative merits of the two methods [*Anderson*, 1984]. This allows flexible use of Anderson's improved FHT or Chave's quadrature method. To verify the forward computation, we compare the magnitude of the seafloor electric field as a function of range with the independent normal-mode method of *Flosadóttir* [1990] (Figure 2). The Earth model (model C of Table 1, see discussion later in the text) differs little from that used for a similar comparison using the lowest mode only by *Chave et al.* [1990]. Here, however, good agreement persists to much shorter ranges (due to inclusion of 30 modes of each polarization, rather than just the lowest mode in the earlier comparison) and to longer ranges (due to the improved FHT). The performance of the FHT out to ranges as long as 1000 km is remarkable. Since the FHT can now be used for even the most attenuated signals we model, the computation speed has greatly improved at long ranges. In addition, *Anderson*'s [1989] use of spline interpolation to reduce

the computational burden when many closely spaced ranges are requested (FHT method only) has proved particularly useful when inverting towed-source, stationary-receiver data, involving a near-continuum of ranges. Together with the efficiently computed Earth-model derivative matrix, this now allows inversion of the full set of source-receiver spacings in experiments where this was previously too computationally intensive (e.g., the inversion example below and the companion paper [*Constable and Cox*, this issue]).

Sensitivity Computation

Fréchet kernels for the seafloor dipole-dipole problem were presented by *Chave* [1984] (for additional references on Fréchet derivatives and sensitivity analysis in layered models, see, for example, *Zhdanov and Keller* [1994, Chapter 9]). *Chave* [1984] used a predictor-corrector method to illustrate Fréchet derivatives for resistive and conductive buried layers. This was used by *Cox et al.* [1983] in a sensitivity study for their seafloor system, but the computations were extremely slow. The approach we use to evaluate the sensitivity matrix is analytical differentiation of the Hankel transform kernels followed by numerical integration [e.g., *Johansen*, 1975; *Constable et al.*, 1987]. Briefly, the kernel k_0 is obtained by a recursion rule of the type $k_0 = k_0(k_1(\cdots k_{\text{underlying half space}}))$, where the seafloor layers are numbered downward and k_l is the kernel computed as if layer l were the uppermost layer. When model-parameter derivatives are required, we save the quantities

$$C_l = \frac{\partial k_0}{\partial k_1}\frac{\partial k_1}{\partial k_2}\cdots\frac{\partial k_{l-1}}{\partial k_l}, \quad l = 1, 2, \cdots, \tag{1}$$

during the forward computation. Afterward, the derivative of the kernel with respect to any model-parameter, call it p_l, (either the thickness or conductivity of layer l) may be obtained from

$$\frac{\partial k_0}{\partial p_l} = C_l\frac{\partial k_l}{\partial p_l}. \tag{2}$$

The electric field derivative follows from the Hankel transforms of $\partial k_0/\partial p_l$ by the same rule used to construct the undifferentiated field from k_0, with a few additional terms due to any dependence of this rule on p_l. The entire Jacobian matrix is returned as a byproduct of a single forward calculation. Since many quantities need be evaluated only once for the entire matrix, very significant computation savings result.

We test our analytical Earth-model derivatives by comparing with finite difference derivatives (Figure 3). The best agreement occurs where the step size is small enough for the first order Taylor approximation error to be small, but before numerical cancellation has become severe [e.g., *Gill et al.*, 1981, p. 127 ff., p. 341 ff.]. Agreement to 5–10 digits is obtained for all data and parameters we have tested. Satisfactory stability of the recursion relations used in the analytical derivative calculation is indicated by the fact that we have subdivided the Earth models into as many as 64 layers without apparent deterioration of the derivatives (e.g., Figure 7).

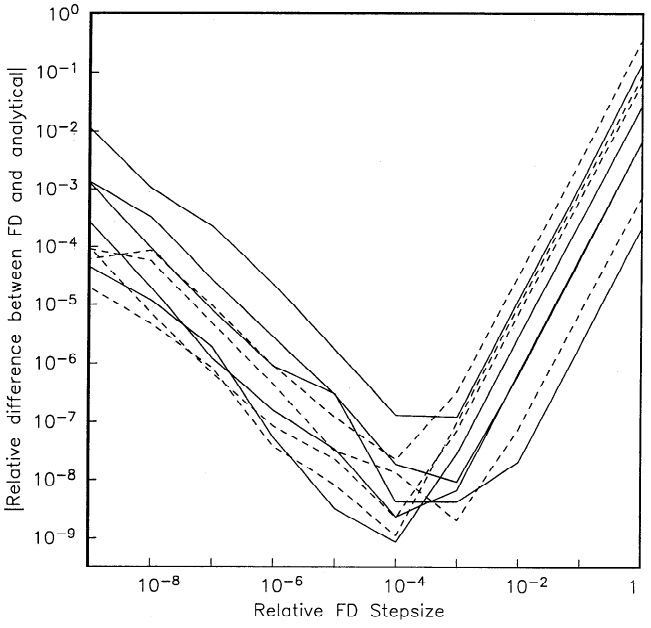

Figure 3. Derivatives from the fast Hankel transform compared with finite differences. The abscissa is the relative finite difference step size used for a central difference derivative evaluation. The ordinate is the magnitude of the relative difference between the finite difference derivative of the complex radial electric field with respect to a model parameter and the same derivative evaluated analytically under the Hankel transform integral sign. The power of ten indicates the number of digits in agreement between the two methods. The Earth model is a 6-layer version of model C, source as in Figure 2; source-receiver distance is 20 km at 45° angle with the transmitter axis. Solid lines are layer-conductivity derivatives. Broken lines are layer-thickness derivatives, for each of the finite layers in the model.

Example of Use for Regularized Data Inversion

The computational time saved with our code is perhaps best shown in the context of the inversion of an actual data set. This also provides confirmation that the Earth-model derivatives are good enough to lead to an acceptable inversion result. Figure 4a shows a data set from the experiment at 13°N on the East Pacific Rise (EPR), described by *Evans et al.* [1991, 1994]. There are 68 data at two frequencies. The large number of layers in regularized inversion produces a large number of columns in the Jacobian matrix. The combination of a towed transmitter with stationary receivers produces a large number of data having unique source-receiver spacings (ranges) and azimuths (with respect to the source axis), so that the number of rows can also be large, and, because the problem is nonlinear, the Jacobian matrix changes at each iteration. Evans et al. used an earlier version of our code which did not incorporate the spline interpolation for range. They made the problem tractable by taking averages of data over a small number of range bins. The small variation in azimuth and the apparently 1-D structure of the upper crust in this experiment made this approach possible, but the EPR study was unusual in this respect.

An inversion of the full data set is shown in Figure 4b. The model consists of 29 layers, so a total of about 2000 partial derivatives were required for each iteration. Anderson's FHT operates efficiently if an array of ranges are provided for computation, but the azimuth of the receiver with respect to the transmitter dipole must remain fixed. To be able to take advantage of the spline interpolation for closely spaced ranges, we perform the calculation for a fixed azimuth (45°) and afterward, outside the forward module, apply a trigonometric transformation to obtain the radial and azimuthal field components for each datum. The entire calculation takes on the order of a minute on average workstations in use at the time of writing, the 2000-

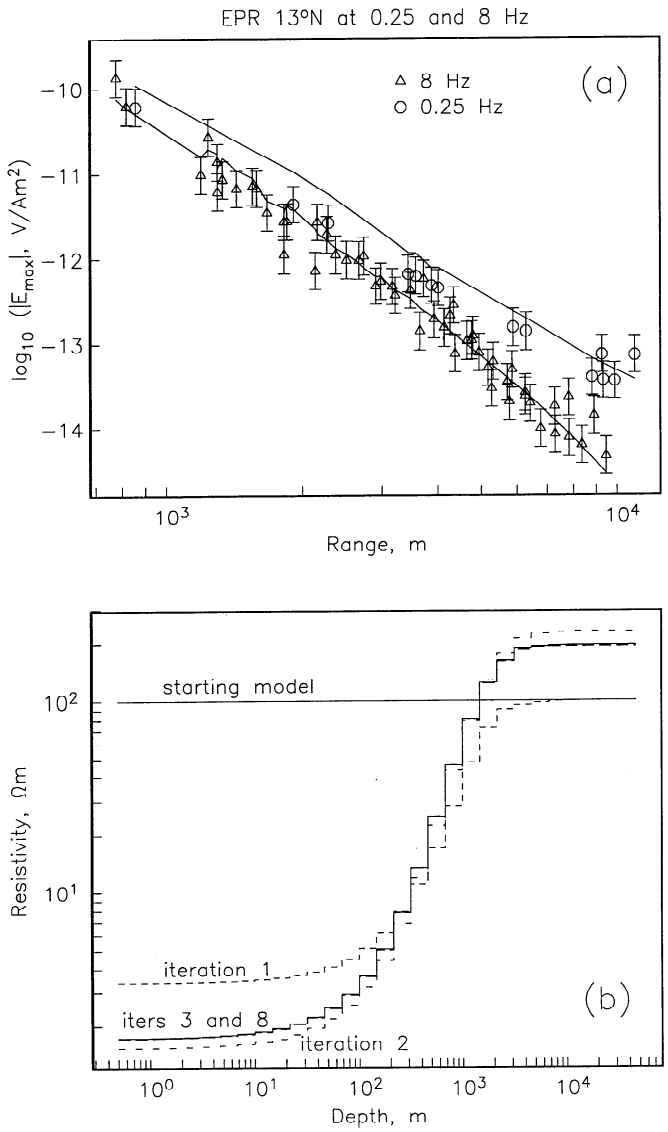

Figure 4. (a) Seafloor EM data taken from the East Pacific Rise on-axis sounding described by *Evans et al.* [1991, 1994]. Data are the amplitudes of the maximum axis of the polarization ellipse. Data errors have been taken at a fixed 50%, to allow for scatter associated with surface heterogeneity. Solid lines are the responses of the converged model shown in the bottom panel. Kinks in this response are due to variations in azimuth for each datum, not represented in this plot. (b) The 29-layer Occam inversion of data shown in Figure 4a. By the third iteration the model has almost reached the converged solution, represented here by the eighth iteration.

derivative computation taking only about a factor of 5 longer than a forward-only computation. The results of this inversion are used both for the crustal model in the next section and in the companion paper [*Constable and Cox*, this issue].

Sensitivity Analysis and Experimental Design

We now illustrate some uses of the sensitivity matrix combined with selected forward calculations. Two models that we consider representative of the uncertainty discussed in the introduction are shown in Table 1 and Figure 5. In order to keep the differences between the models as simple as possible, the crustal sections are identical. The structure of the volcanic crustal sequence is based on inversions of the East Pacific Rise controlled-source experiment (see the preceding section and *Evans et al.* [1994]), preliminary inversions of the PEGASUS experiment (on 40-Ma lithosphere in the NE Pacific) [*Constable and Cox*, this issue], and on borehole logging [*Becker et al.*, 1982; *Becker*, 1985]. Sediment thickness varies greatly on the ocean floor. Here we assume the average thickness at the PEGASUS site [*Constable and Cox*, this issue]. The sediment conductivity assumed makes little difference at the frequencies we discuss here. In the uppermost mantle, model C is similar to the Pacific reference model of *Chave et al.* [1990], representative of the uppermost mantle conductivities found in MT inversions. The lithospheric profile of model R is based on 40-Ma subsolidus olivine profiles presented by *Heinson and Constable* [1992]. The lowest conductivity has been increased (such an increase might be due to a percentage of water or trace materials limiting the resistivity of cold mantle rock) as needed to yield the same lithospheric transverse resistance of $3 \times 10^9\ \Omega\ m^2$.

Forward Response

We begin by looking at a view of the magnitude of the seafloor electric field over model C as a function of range and frequency (Figure 6). The field has been normalized to represent a unit source strength, so that a contour labeled "−17" (indicating a normalized field magnitude of 10^{-17} V/m) corresponds to the lowest signal levels detected in experimental work to date. The ranges and frequencies included in Figure 6 are a generous estimate of the usable part of data space. However, this domain was chosen to delineate the intrinsic limits to experimental sensitivity, while the limitations imposed by realistic noise models are left to a later section. The forward response shows three distinct regimes:

1. At short ranges and all but the highest frequencies, the signal is dominated by a frequency-independent r^{-3} range dependence associated with the geometry of a dipole over a half-

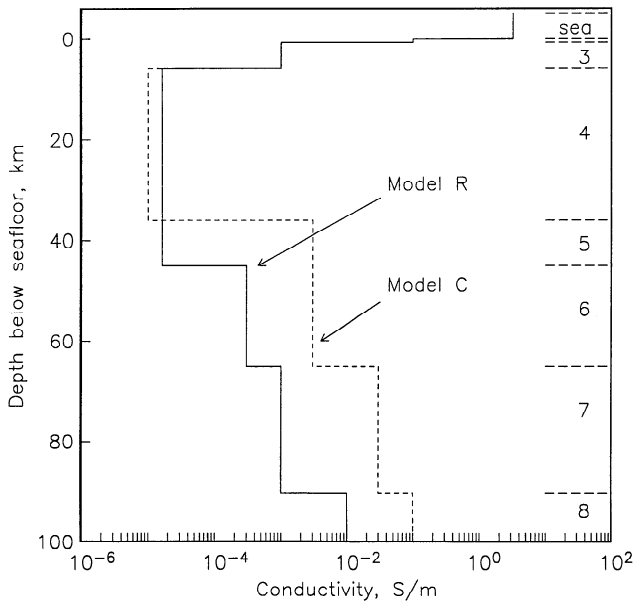

Figure 5. Earth conductivity models, model R based on the 40 Ma model of *Heinson and Constable* [1992] and model C, similar to the model of *Chave et al.* [1990].

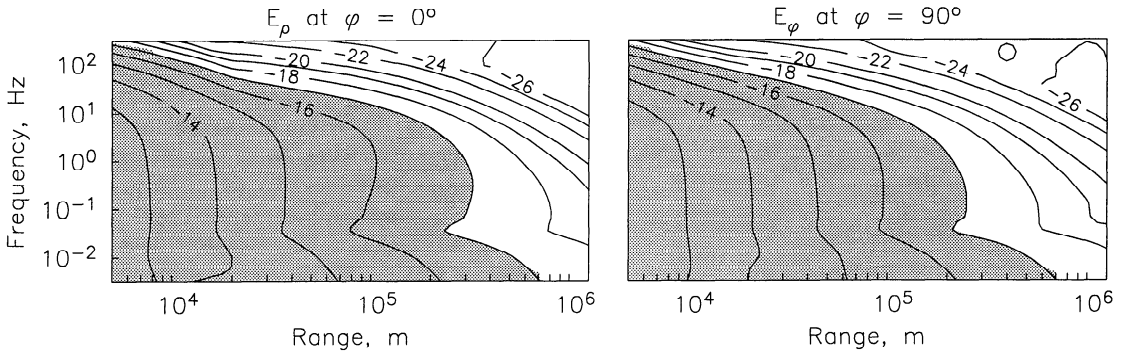

Figure 6. Magnitude of the radial (E_ρ, left) and azimuthal (E_ϕ, right) electric field just above the seafloor for a unit HED source over model C. The horizontal axis represents source-receiver distance ranging between 5 km and 1000 km, and the vertical axis represents transmitter frequency between 0.01 and 100 Hz. In the left-hand panel, the source-receiver distance is measured along a line extending off the transmitter axis, and the 10-logarithm of the magnitude of the radial electric field component is contoured. In the right-hand panel the horizontal axis represents distance along a line broadside to the transmitting dipole, and the azimuthal electric field component is contoured.

space. This is manifest as vertical contours at frequencies where there is no skin-depth attenuation.

2. For ranges greater than a few tens of kilometers, propagation is dominated by the "down-over-up" path of least attenuation [e.g., *Baños*, 1966; *Kraichman*, 1970; *Wait*, 1971; *Galejs*, 1972; *Frieman and Kroll*, 1973; *Brekhovskikh*, 1980], down through the crustal section, laterally along the mantle resistor, and up to the receiver. Such a signal is characterized by a range-independent prefactor, set by the "down" and "up" parts of the path and by an r^{-2} geometric effect times exponential decay with skin depths along the deeper, more resistive layers. Since the logarithm of the field strength is contoured, the slope of the contours should be approximately proportional to $-r/\sqrt{(\sigma f)}$. This frequency dependence explains the increase in slope at lower frequencies.

3. At the lowest frequencies, another, much less range-dependent mechanism takes over. This is closely related to the sea surface, as may be demonstrated by varying the water depth (Figure 6 assumes a 5-km water depth). The code includes the effect of the sea/air boundary and an atmosphere of zero conductivity. At most frequencies, attenuation in the seawater is far too great for signals reaching the sea surface to have any significance at the sea floor. By 10^{-2} Hz, however, there are only 3.7 skin depths to the sea surface and back. The contours show a rapid change in slope near this frequency. When the sea surface signal begins to dominate over the seabed propagation path, the sensitivity to the seabed structure is lost. In contrast with magnetotelluric and other ambient noise sources which begin to limit signal reception at these frequencies, the sea surface limitation cannot be circumvented by any amount of source strength or stacking time. The "notch" that develops at ranges greater than 10 km and frequencies around 0.03 Hz is probably a result of phase cancellation between the sea surface and lithospheric paths.

Sensitivity Overview Plots

The layered-Earth derivatives can be used to plot a discrete equivalent of the Fréchet derivative. In Figure 7, the triangles and solid lines show results from subdividing each layer into 5 and 10 sublayers, respectively.

For a broader overview of the sensitivity to the Earth model, Figure 8 shows separate panels for each of the Earth-model parameters of model R over a large range of frequencies and source-receiver separations. The quantity plotted is

$$S \equiv \frac{\partial(\ln(d))}{\partial(\ln(p))} = \frac{p}{d}\frac{\partial d}{\partial p} \tag{3}$$

where the datum d is taken to be the magnitude of an electric field component and the Earth-model parameter p can be either

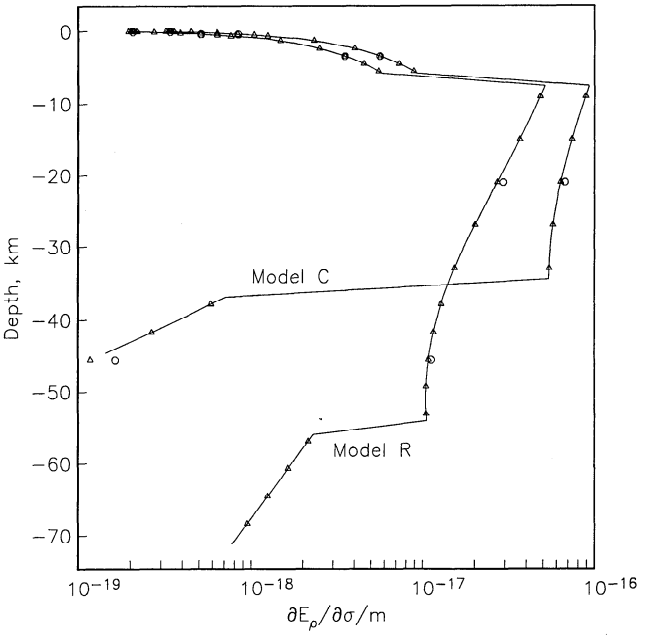

Figure 7. Discrete analog of the Fréchet derivative in Earth models C and R. The horizontal axis is the derivative of the magnitude of the radial electric field with respect to a layer conductivity, divided by the layer thickness. The source is a unit strength HED transitting at 1 Hz, receiver located 100 km from the source, in line with the transmitter axis (radial component). Circles indicate layering as in Table 1. Triangles indicate each layer subdivided into 5 sublayers. Solid lines indicate each layer subdivided into 10 sublayers.

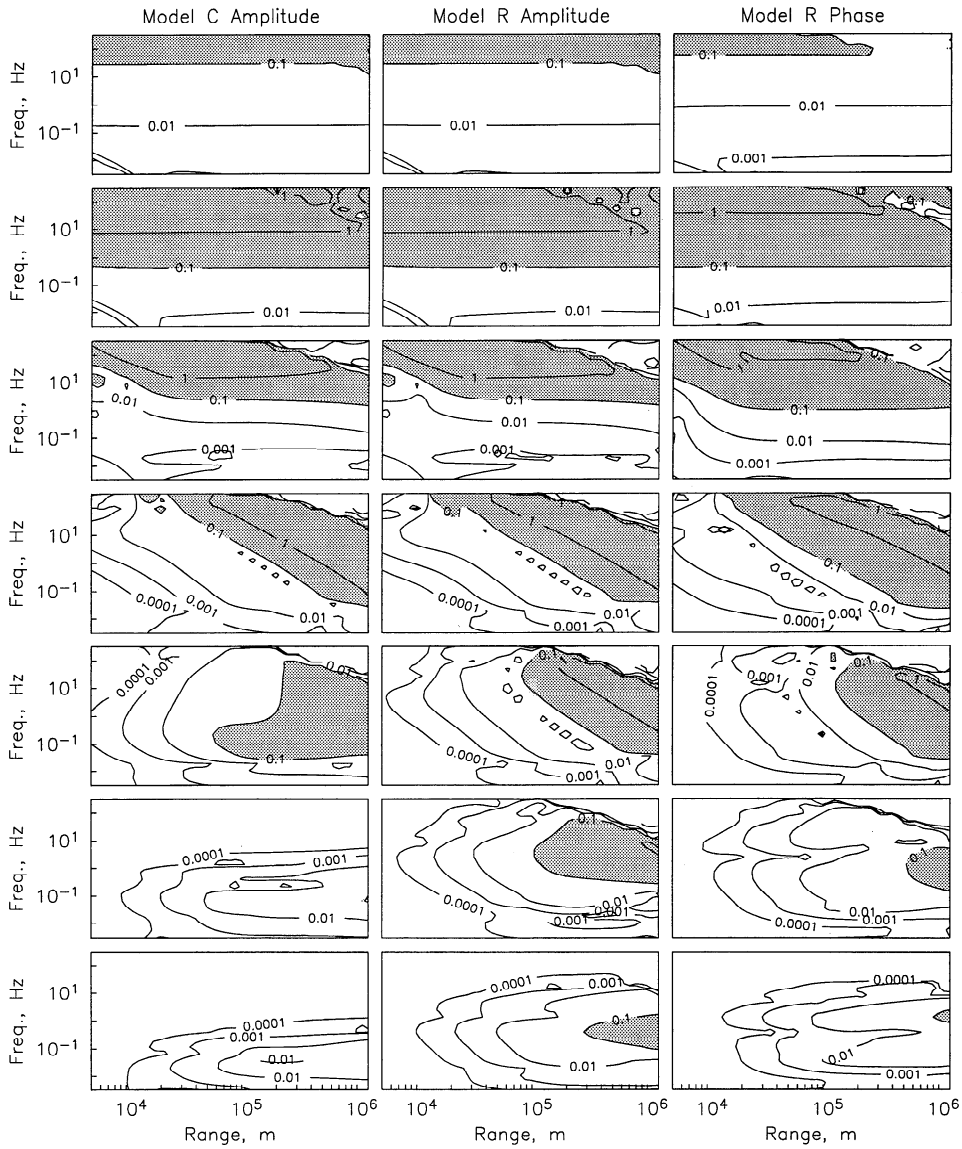

Figure 8. Overview of the sensitivity of the magnitude of the HED radial electric field over models C and R (see Table 1) and phase for model R only. In the amplitude plots, the quantity contoured is $S \equiv \partial(\ln(d))/\partial(\ln(p)) = p\partial d/d\partial p$, where the datum is $d = |E_\rho(r, f)|$, the magnitude of the radial electric field evaluated slightly above the seafloor, and r represents distance along a line extending off the source dipole axis. For the phase, we contour $S \equiv 0.5\ \partial(\ln(d))/\partial(\ln(p)) = p\partial d/d\partial p$, where $d = \arctan(\mathrm{Im}[E_\rho(r, f)]/\mathrm{Re}[E_\rho(r, f)])$. Each panel represents the conductivity of a single layer, from the sediment layer (top panels), down to the layer immediately above the underlying half-space (bottom panels). (Sensitivity to the half-space conductivity is low and has been omitted for clarity.) A value of $S = x$ means that if the conductivity σ were perturbed by factor f, the datum would change by factor f^x.

a layer conductivity or thickness. A value of $S = 1$ means that if the parameter p is perturbed by factor f, the datum changes by the same factor. For $S = 2$, the datum would change by factor f^2.

Some justification of our choice of logarithmic scaling for both the data and the model parameters may be appropriate. The primary reason is for simplicity and to be able to view a large amount of information on one page. In specific cases, it may be more appropriate to ask what is being sought. For instance, seeking porosities through Archie's Law with exponent 2, then $\sqrt{\sigma}$ rather than $\log(\sigma)$ might be appropriate. Of course, the Archie relationship could be used to compute sensitivities with respect to porosities directly; once $\partial d/\partial\sigma$ is available, any derived quantity can readily be found using the chain rule. Another reason to use logarithmic scaling is that this is appropriate for comparing sensitivity with relative experimental errors.

Figure 8 contains a wealth of information about the physics of the seafloor HED method:

1. As in Figure 7, the physics of the down-across-up path are evident. Derivatives for the three crustal layers, in which propagation is mostly down and up, are largely independent of range (the irregular patterns in the upper right-hand corner of Figure 8 result from breakdown of the numerical integration at very low signal levels) and only reflect changing attenuation with

frequency, high frequencies having the largest effect. Layers 4 and 5, on the other hand, show the combined effect of range and frequency, with 2 orders of magnitude of frequency having the same effect as 1 order of magnitude of range because of the $\sqrt{f}$ dependence of skin depth. Deep conductive layers (5–8 in C and 6–8 in R) show a largely range-dependent behavior limited to the band of frequencies that can penetrate to these depths. This reflects cumulative losses from the bottom of the resistive "waveguide".

2. For simplicity, we have plotted only the magnitude of the derivatives. For large magnitudes (dark areas), the derivatives are negative (increasing conductivity attenuates the signal). However, the diagonal beads of closed contours in layers 4 and 5 and the horizontal notches in deeper layers, indicate where the derivatives change sign. For layer 6 of model R most of the derivatives are positive, demonstrating that, as shown by the forward calculations of *Chave et al.* [1990], providing a conductive mantle at the base of the waveguide will actually increase signal amplitude.

3. For the purpose of distinguishing models C and R, we are most interested in layer 5, the lithospheric layer corresponding to depths between 36 and 55 km. Here we find the greatest sensitivity at the longest ranges and at frequencies between roughly 1 and 10 Hz. There is a significant difference between the sensitivity of the two models to this layer. Model C is underlain by a strong conductivity gradient which enhances its long-range signal, while lower layers of model R resemble a half-space, losing more of its energy into the mantle. Evidently, R is more sensitive to the introduction of a deep conductivity gradient than C is to changes in its details. The shape of the sensitivity contours shows that the PEGASUS experiment's [*Constable and Cox*, this issue] emphasis on reaching long ranges at a frequency near 8 Hz was a good choice. Near that frequency, the darkest shade, which corresponds to $S = 1$, or to a relative change in the response equal or larger than the relative conductivity perturbation, comes as close as ~200 km for model R. At a range of ~100 km, the value of S = 0.3 would translate a factor 2 change in this layer's conductivity to a signal change of $2^{0.3}$ or 23%. As the experimental paper [*Constable and Cox*, this issue] will show, with a single instrument at the longest range of ~80 km the PEGASUS experiment came close but did not quite manage to distinguish the two types of models.

4. The relative unimportance of the surface sediments at the frequencies considered can be seen by the small values of the derivatives for layer 1.

5. As noted by *Constable et al.* [1986], the derivatives of the phase are very similar to the derivatives of amplitude. Although not shown, the derivatives with respect to layer thickness mimic the form of the conductivity derivatives.

6. Spatial aliasing of the signal caused by variations in the uppermost layers has the potential to confuse interpretation of the deeper parts of the profile, as has been discussed by *Unsworth* [1994] and *Unsworth and Oldenburg* [1995]. Figure 8 shows well-separated regions sensitive only to shallow crust parameters or only to the mantle parameters, implying that at least for this one-dimensional structure it is in principle possible to resolve surficial and deep structure independently. In a later section, we will discuss a statistical approach to the very real problem of near-surface heterogeneity.

Effect of Noise on Experimental Design

Inferences from model sensitivities involve extrapolation from infinitesimal model perturbations. Since Earth conductivity is often unknown to orders of magnitude, it is clearly important to confirm such inferences by selected forward computations. Furthermore, neither Earth model derivatives nor differences between theoretical forward curves have much meaning unless they are carefully weighed against the experimental limitations. We will consider two types of limitations; a detection threshold (i.e., whether a signal is large enough to emerge from a noise background) and noise more or less proportional to the signal strength.

At the typical controlled-source frequencies within a decade or two of 1 Hz, the deep seafloor is electrically a very quiet environment. Above about 1 Hz, the main source of noise is caused by the receiving equipment [*Webb et al.*, 1985] rather than ambient noise levels. Receiver sensitivity may be increased by increasing antenna length, producing a larger recorded voltage for a given electric field. Synchronous stacking can also be used to recover a repetitive signal from a random background of either instrumental or natural ambient noise. Because transmitter power, stacking time (or bandwidth), and receiver antenna length are all under the control of the experimenters, no absolute limit on the detection threshold above 1 Hz has been reached. The best accomplished to date is about 10^{-17} V/Am^2 using a 3-km antenna on a long-wire electromagnetic (LEM) type receiver [*Constable and Cox*, this issue]. The shorter arms on the other electric field (ELF-type) instruments reduce this to about 10^{-15} V/Am^2. For evaluating the differences between the response to our two models, we use an instrumental and ambient noise spectrum based on Figure 7 of *Webb et al.* [1985]. The instrumental part of the noise spectrum (including electrode noise) is taken to vary as f^{-1}, leveling out above 1 Hz at a value of 10^{-12} (V/m)/$\sqrt{\text{Hz}}$ for the case of a 1000-m antenna. At lower frequencies, first ionospheric and then ocean-induced fields begin to contaminate seafloor electric dipole-dipole sounding sig-

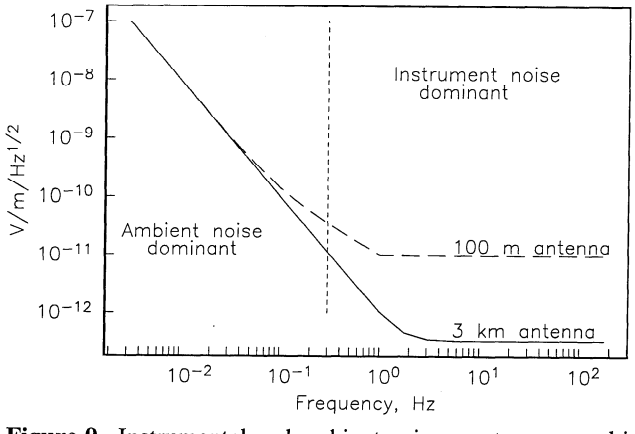

Figure 9. Instrumental and ambient noise spectra assumed in our comparisons of model response. The spectra are based on experimental results reported in Figure 7 of *Webb et al.* [1985]. Instrumental (including electrode) noise is taken to produce a voltage independent of the receiver antenna length, so that when this is interpreted as an electric field value, it scales with the reciprocal of the antenna length. The two lengths shown correspond to the two noise models discussed later in the text and used in the middle and bottom panels of Figure 10. This part of the noise spectrum is taken to vary as f^{-1}, leveling out above 1 Hz at a value of 1.0×10^{-12} (V/m)/$\sqrt{\text{Hz}}$ in the case of a 1000 m antenna. The ambient noise spectrum is taken to vary as f^{-2} throughout the frequency range, passing through a value of 10^{-10} (V/m)/$\sqrt{\text{Hz}}$ at 0.1 Hz.

nals. To model this, the ambient noise spectrum is taken to vary as f^{-2} throughout the frequency range shown, passing through a value of 10^{-10} (V/m)/$\sqrt{\text{Hz}}$ at 0.1 Hz. Figure 9 shows the combination of these two sources of noise for two different antenna lengths.

In addition to the instrumental and ambient sources of noise, errors more or less proportional to the signal strength also need to be considered. Because of the very sharp falloff of electric field with range (on the order of $1/r^3$ for short ranges and e^{-r} at long ranges), there are ordinarily very few data for which instrument noise is comparable to the size of the signal; most are either below the detection threshold or have an extremely high signal to instrument noise ratio. For those data above the detection threshold, instrumental error rapidly becomes only a few percent or less and ceases to be the most important source of noise. From the interpretational standpoint, uncertainty in source-receiver range, transmitter azimuth, and receiver orientation all contribute random errors which are larger than this. However, the dominant source of measurement degradation over thinly sedimented seafloor is data scatter believed to be related to near-surface geological structure and topography [*Cox et al.*, 1986; *Evans et al.*, 1994]. Inspection of Figure 4a provides an illustration; the data scatter about the theoretical response and the error bars have to be set at 50% of the electric field magnitude before an adequate fit can be obtained using inverse modeling. These data were collected from two receivers and from four transmitter paths which spanned ranges from 500 m to 10 km. Although crustal heterogeneity is, in principle, deterministic in the sense that it could be included by a sufficiently complex modeling algorithm, the scatter exhibits all the characteristics of random noise. That is, there is no correlation between data collected at adjacent ranges, and there is no trend or bias in the layered-seafloor fit as a function of range (except for a few 0.25 Hz data at 2- to 4-km range). Examination of the electric field magnitude and phase during this experiment showed that fluctuations occurred on the same scale lengths as the transmitter antenna length, or 100 m. Each datum in Figure 4 is the result of 15-min synchronous stacking of the transmitter signal, during which time the transmitter antenna was towed about 500 m, or 5 times its length. Thus even for a similar receiver and transmitter path, the near-surface structure has an essentially independent effect on adjacent data.

The example just discussed is an extreme case, at relatively short ranges over fresh volcanic terrain; the effect is reduced over sediments and at longer ranges [*Constable and Cox*, this issue]. Even so, a 50% error level for individual data is not as grave a problem as it may seem. With multiple receivers and a towed source or with tandem-towed source-receiver systems, it is easy to obtain redundant data and use some form of averaging to reduce the scatter associated with surface heterogeneity. *Evans et al.* [1991] reduced the error on each datum in the example data set to 10%–20% by taking groups of data in range bins and computing the standard error of the mean for each bin. The measurement error estimates were discarded and only the variance in each range bin was used for the error calculation. This approach was made possible by the apparently 1-D response in this short-range experiment and by an experimental design which resulted in very little azimuth variation. It proved self-consistent for this data set in the sense that 1-D models could easily be fit at a root-mean-square misfit level of 1.0. However, the method is not generally applicable, since azimuths relative to the transmitter dipole may vary freely. Also, the choice of bin boundaries can have a significant effect on the outcome. With the efficient modeling algorithm presented here, all of the mostly redundant data can be included in inversion. The effective data error is then given by the square root of the variance of fit at convergence, which goes as $1/\sqrt{N}$ where N is the number of data with independent transmitter and receiver locations [e.g., *Bevington*, 1969]. With a towed source, collecting on the order of 100 data per decade of range will generally be possible (the EPR example had a relatively short transmission time). With multiple receivers, an effective error level of 5% seems very reasonable. Over thickly sedimented structures, the scatter will be much less, but other experimental parameters, especially the strong dependence on range, will contribute to random error and likely bring the effective error back into the 5% level. Also, large-scale deviations from 1-D structure are likely to affect the data at least this much.

In the next section, we will model noise for two different types of experiments. The first case considered represents an experiment where the emphasis has been put on reducing scatter due to near-surface geology and other relative "noise" by collecting large numbers of redundant data. The easily deployed ELFs with 10-m receiving antennas would be the first choice for such an experiment but do not provide strong enough signals, so we show results for 100-m antennas and assume a relative error of 5%. We also assume a source strength of 3.6×10^4 Am and stack time of 15 min, typical of towed-source experiments to date. The second case we consider is an experiment where more emphasis has been put on receiving weak signals than on gathering redundant data. We assume a receiver antenna length equal to the longest achieved to date, 3 km, and since we are trying to illustrate an extreme case, assume a very long stack time of 12 hours. While signals over 12 hours were stacked for one of the instruments in the PEGASUS experient [*Constable and Cox*, this issue], such stack times are perhaps more appropriately viewed as an example of what could be done with moored or island sources rather than towed sources (C.S. Cox, personal communication, 1983). In keeping with the emphasis on receiving weak signals, we assume a somewhat stronger transmitter than in the previous noise model, or 1.0×10^5 Am, but lack of redundant data implies a larger relative error of 20%. Both noise models assume numbers that have been already been achieved with current technology. Technological advances (for instance improvements in electrode construction (C.S. Cox and X. Qian, personal communication, 1993) or increased experimental resources may well make it possible to go beyond these boundaries.

Can the Two Models Be Distinguished?

The top panels of Figure 10 show the forward response of models R and C. The lower panels show the difference in field magnitude, scaled by the estimated noise levels for the two types of experiments discussed above. The results are fairly similar, even though the middle and bottom panels involve 5% and 20% relative noise, respectively. In both cases, for frequencies between roughly 1 and 10 Hz, at least for the radial field component, the differences between the models reach twice the noise level at ranges of the order of 100 km. This should be sufficient to distinguish the two models experimentally. The PEGASUS experiment, with its emphasis on reaching long ranges at 8 Hz, was clearly well designed for this purpose. As the companion paper [*Constable and Cox*, this issue] shows, however, while differences in fit are beginning to show up at the longest ranges, both models more or less fit the data after minor adjustments to the crustal profile. Our conclusion from both the model and

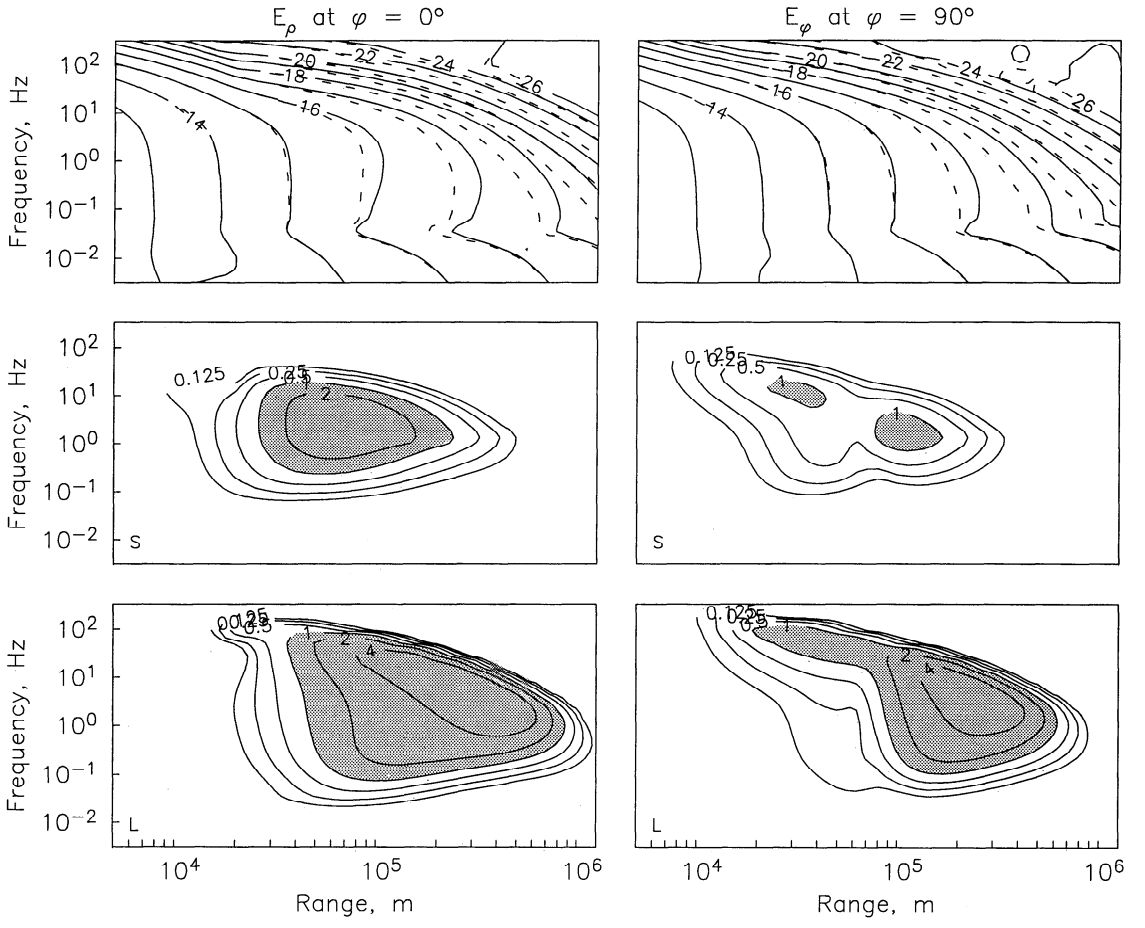

Figure 10. Forward calculations and noise-scaled differences testing sensitivity to the difference between mantle models R and C. As in Figures 5 and 7, the horizontal axis is HED source-receiver distance between 5 and 1000 km, and the vertical axis is transmitter frequency between 0.01 and 100 Hz. In the left-hand panels, the receiver is assumed to be located along a line oriented at endfire relative to the transmitting dipole, and we consider the radial component of the seafloor electric field. The right-hand panels are similar to those on the left, except that the receiver is assumed to be located along a line broadside to the transmitter, and we consider the azimuthal field component. The top panels show the forward response of models R (solid) and C (broken). In the lower two panels, we contour the difference of the electric field in the two Earth models, divided by an estimated noise level. In the middle panels, the noise level is given by the 100-m antenna curve of Figure 9, plus 5% relative noise. In the bottom panels, the noise level is that of the 3-km antenna curve of Figure 9, plus 20% relative noise.

the experimental study is that the ranges reached stopped just short of beginning to distinguish between the two types of models, and, that in experiments using current technology, ranges only need to be pushed slightly further to distinguish the differences between a thinner, more resistive lithospheric resistor layer underlain by a deeper conductivity gradient, such as the one in model C, and a thicker, less resistive layer, as in model R. This is the case even for our relatively minor model differences, identical transverse resistance, and in the presence of reasonably realistic noise models.

Acknowledgments. The authors thank A.D. Chave and W.L. Anderson for providing their codes and C.S. Cox and S.C. Webb both for collaboration on experimental work and for many useful discussions. We thank R.N. Edwards, P.E. Wannamaker, and M.S. Zhdanov for reviews which have improved the manuscript and R. Parker for the plotting programs Plotxy, Contour, and Color, used for most of the figures in this paper. A.F. thanks J.C. Larsen for his support while at PMEL. The East Pacific Rise work was done by S.C. in collaboration with M.C. Sinha, M.J. Unsworth, and R.L. Evans. S.C. acknowledges financial support from the NSF and A.F. from a NATO Science Fellowship.

References

Anderson, W.L., Numerical integration of related Hankel transforms of orders 0 and 1 by adaptive digital filtering, *Geophysics*, *44*, 1287–1305, 1979.

Anderson, W.L., Discussion of: Numerical integration of Hankel transforms by quadrature and continued fraction expansion, by A.D. Chave (with reply by the author), *Geophysics*, *49*, 1811–1813, 1984.

Anderson, W.L., A hybrid fast Hankel transform algorithm for electromagnetic modeling, *Geophysics*, *54*, 263–266, 1989.

Baños, A., *Dipole Radiation in the Presence of a Conducting Half-Space*, Pergamon, Tarrytown, N.Y., 1966.

Becker, K., Large-scale electrical resistivity and bulk porosity of the oceanic crust, Deep Sea Drilling Project Hole 504 B, Costa Rica Rift, *Initial Rep. Deep Sea Drill. Proj.*, *83*, 419–427, 1985.

Becker, K., et al., In situ electrical resistivity and bulk porosity of the oceanic crust, Costa Rica Rift, *Nature*, *300*, 594–598, 1982.

Bevington, P.R., *Data Reduction and Error Analysis for the Physical Sciences*, McGraw-Hill, New York, 1969.

Brekhovskikh, L.M., *Waves in Layered Media*, 2nd ed., Academic, San Diego, Calif., 1980.

Chave, A.D., Numerical integration of Hankel transforms by quadrature and continued fraction expansion, *Geophysics*, *48*, 1671–1686, 1983.

Chave, A.D., The Fréchet derivatives of electromagnetic induction, *J. Geophys. Res.*, *89*, 3373–3380, 1984.

Chave, A.D., and C.S. Cox, Controlled electromagnetic sources for measuring electrical conductivity beneath the oceans, 1, Forward problem and model study, *J. Geophys. Res.*, *87*, 5327–5338, 1982.

Chave, A.D., Á. Flosadóttir, and C.S. Cox, Some comments on seabed propagation of ULF/ELF electromagnetic fields, *Radio Sci.*, *25*, 825–836, 1990.

Chave, A.D., S.C. Constable, and R.N. Edwards, Electrical exploration methods for the seafloor, in *Electromagnetic Methods in Applied Geophysics,* vol. 2, edited by M. Nabighian, pp. 931–966, Soc. of Explor. Geophys., Tulsa, Okla., 1991.

Constable, S., Marine electromagnetic induction studies, *Surv. Geophys.*, *11*, 303–327, 1990.

Constable, S., and G.S. Heinson, In defense of a resistive oceanic uppper mantle: Reply to a comment by Tarits, Chave and Schultz, *Geophys. J. Int.*, *114*, 717–723, 1993.

Constable, S., and C.S. Cox, Lithospheric structure from marine controlled-source electromagnetic sounding 2. The PEGASUS experiment, *J. Geophys. Res.*, this issue.

Constable, S.C., C.S. Cox, and A.D. Chave, Offshore electromagnetic surveying techniques, paper presented at 56th Annual International Meeting, Soc. for Explor. Geophys., Houston, Tex., 1986.

Constable, S., R.L. Parker, and C.G. Constable, Occam's inversion: A practical algorithm for generating smooth models from electromagnetic sounding data, *Geophysics*, *52*, 289–300, 1987.

Cox, C.S., Electromagnetic induction in the oceans and inferences on the constitution of the Earth, *Geophys. Surv.*, *4*, 137–156, 1980.

Cox, C.S., J.H. Filloux, and J. Larsen, Electromagnetic studies of ocean currents and electrical conductivity below the ocean floor, in *The Sea,* vol. 4, part I, edited by A.E. Maxwell, pp. 637–693, John Wiley, New York, 1971.

Cox, C.S., A.D. Chave, S.C. Constable, and G. Sasagawa, Model studies of an ocean-bottom electrical sounding experiment (abstract), *Trans. AGU*, *64*(45), 692, 1983.

Cox, C.S., S.C. Constable, A.D. Chave, and S.C. Webb, Controlled-source electromagnetic sounding of the oceanic lithosphere, *Nature*, *320*, 52-54, 1986.

Edwards, R.N., and A.D. Chave, A transient electric dipole-dipole method for mapping the conductivity of the sea floor, *Geophysics*, *51*, 984-987, 1986.

Edwards, R.N., L.K. Law, and J.M. DeLaurier, On measuring the electrical conductivity of the oceanic crust by a modified magnetometric resistivity method, *J. Geophys. Res.*, *86*, 11,609–11,615, 1981.

Evans, R.L., S.C. Constable, M.C. Sinha, C.S. Cox and M.J. Unsworth, Upper crustal resistiviey structure of the East Pacific Rise near 13°N, *Geophys. Res. Lett.*, *18*, 1917–1920, 1991.

Evans, R.L., M.C. Sinha, S.C. Constable and M.J. Unsworth, On the electrical nature of the axial melt zone at 13°N on the East Pacific Rise, *J. Geophys. Res.*, *99*, 577–588, 1994.

Everett, M.E., and R.N. Edwards, Electromagnetic expression of axial magma chambers, *Geophys. Res. Lett.*, *16*, 1003–1006, 1989.

Everett, M.E., and R.N. Edwards, Transient marine electromagnetics: The 2.5-D forward problem, *Geophys. J. Int.*, *113*, 545–561, 1993.

Filloux, J.H., Instrumentation and experimental methods for oceanic studies, in *Geomagnetism,* vol. 1, edited by J.A. Jacobs, pp. 143–246, Academic, San Diego, Calif., 1987.

Flosadóttir, A.H., The response of the oceanic lithosphere to electromagnetic controlled source transmitters modeled using local spectral representation, *SIO Ref. Ser.*, *90*, 228 pp., Scripps Inst. of Oceanogr., La Jolla, Calif., 1990.

Frieman, E.A., and N.M. Kroll, Lithospheric propagation for undersea communication, technical report (JMSON), JSS pp. 73–75, Stanford Res. Inst., Menlo Park, Calif., 1973.

Galejs, J., *Terrestrial Propagation of Long Electromagnetic Waves*, Pergamon, Tarrytown, N.Y., 1972.

Ghosh, D.P., Inverse filter coefficients for the computation of apparent resistivity standard curves for a horizontally stratified Earth, *Geophys. Prospect.*, *19*, 769-775, 1971.

Gill, P.E., W. Murray, and M.H. Wright, *Practical Optimization*, Academic, San Diego, Calif., 1981.

Heinson, G., and S. Constable, The electrical conductivity of the oceanic upper mantle, *Geophys. J. Int.*, *110*, 159-179, 1992.

Jattieva, Z., N. Palshin, L. Vanyan, S. Constable, S. Webb and C. Cox, Range-dependent apparent resistivity of the seafloor frequency sounding, paper presented at 7th Assembly, Int. Assoc. of Geomagn. and Aeron., Buenos Aires, Argentina, 1993.

Johansen, H.K., An interactive computer/graphic-display-terminal system for interpretation of resistivity soundings, *Geophys. Prospect.*, *23*, 449–458, 1975.

Kraichman, M.B., *Handbook of Electromagnetic Propagation in Conducting Media*, U.S. Govt. Prin. Offic., Washington, D.C., 1970.

Mackie, R.L., B.T. Bennett, and T.R. Madden, Long-period magnetotelluric measurements near the central california coast: A land-locked view of the conductivity structure under the Pacific Ocean, *Geophys. J.*, *95*, 181-194, 1988.

Ranganayaki, A.P., and T.R. Madden, Generalized thin sheet analysis in magnetotellurics: an extension of Price's analysis, *Geophys. J. R. Astron. Soc.*, *60*, 445–457, 1980.

Sinha, M.C., P.D. Patel, M.J. Unsworth, T.R.E. Owen, and M.R.G. MacCormac, An active source electromagnetic system for marine use, *Mar. Geophys. Res.*, *12*, 59–68, 1990.

Smith, J.T., and J.R. Booker, Magnetotelluric inversion for minimum structure, *Geophys. Prospect.*, *53*, 1565–1576, 1988.

Tarits, P., Electromagnetic studies of global geodynamic processes, *Surv. Geophys.*, *15*, 209–238, 1994.

Tarits, P., A.D. Chave, and A. Schultz, Comment on 'The electrical conductivity of the oceanic upper mantle' by G. Heinson and S. Constable, *Geophys. J. Int.*, *114*, 711–716, 1993.

Unsworth, M., Exploration of mid-ocean ridges with a frequency domain electromagnetic system, *Geophys. J. Int.*, *116*, 447-467, 1994.

Unsworth, M., and D. Oldenburg, Subspace inversion of electromagnetic data – application to mid-ocean ridge exploration, *Geophys. J. Int.*, *123*, 161–168, 1995.

Unsworth, M., B.J. Travis and A.D. Chave, Electromagnetic induction by a finite dipole source over a 2-D Earth, *Geophysics*, *58*, 198–214, 1993.

Wait, J.R., Electromagnetic probing in geophysics, in *Theory of Ground Wave Propagation*, Chap. 5, Golem, Boulder, Color., 1971.

Webb, S.C., S.C. Constable, C.S. Cox, and T. Deaton, A seafloor electric field instrument, *J. Geomagn. Geoelectr.*, *37*, 1115–1130, 1985.

Webb, S.C., R.N. Edwards, and L. Yu, First measurements from a deep-tow transient electromagnetic sounding system, *Mar. Geophys. Res.*, *15*, 13–26, 1993.

Young, P.D., and C.S. Cox, Electromagnetic active source sounding near the East Pacific Rise, *Geophys. Res. Lett.*, *8*, 1043–1046, 1981.

Yu, L., and R.N. Edwards, The detection of lateral anisotropy of the ocean floor by electromagnetic methods, *Geophys. J. Int.*, *108*, 433–441, 1992.

Zhdanov, M.S., and G.V. Keller, *The Geoelectrical Methods in Geophysical Exploration*, Elsevier, New York, 1994.

S. Constable, University of California San Diego, Scripps Institution of Oceanography, Institute of Geophysics and Planetary Physics 0225, La Jolla, CA 92093-0225. (e-mail: sconstable@ucsd.edu)

Á.H. Flosadóttir, NOAA/PMEL, Building 3, 7600 Sand Point Way, Seattle, WA 98115-0070. (e-mail: agusta@pmel.noaa.gov)

(Received April 19, 1995, revised November 17, 1995, accepted November 21, 1995.)